# LATERAL VARIATIONS IN BULK DENSITY AND POROSITY OF THE UPPER LUNAR CRUST FROM HIGH-RESOLUTION GRAVITY AND TOPOGRAPHY DATA: COMPARISON OF DIFFERENT ANALYSIS TECHNIQUES

D. Wahl[1], J. Oberst[1,2]

[1] Technische Universität Berlin, Chair of Planetary Geodesy, 10623 Berlin, Germany - daniel.wahl@tu-berlin.de
[2] German Aerospace Center (DLR), Institute of Planetary Research, 12489 Berlin, Germany - juergen.oberst@dlr.de

**Commission III, ICWG III/II**

**KEY WORDS:** Gravity Field, Bouguer Anomalies, Correlation Analysis, GRAIL, LOLA

**ABSTRACT:**

We map lateral variations in bulk density of the upper lunar highland crust using the most recent GRAIL gravity field solution of degree and order 1500 in combination with LOLA topography data, both truncated to an upper limit of degree and order 700. Our maps have a spatial resolution of 0.75°, where each grid point was calculated using circular analysis regions of 3° radius. We apply two methods, which yield similar results for most parts of the study area. The first method minimizes the correlation between topography and Bouguer anomalies, the second maximizes the smoothness of the Bouguer anomalies. Both approaches suffer in the case that terrain is flat and lacks topographic features; consequently, this is where results from the two methods differ. We also mapped porosity of the crust using grain densities derived from Lunar Prospector spectrometry and sample analysis. It appears that variations in bulk density are mostly related to differences in crustal porosity. We find that high porosity is often associated with areas of impact basins. This confirms earlier studies, that impacts changed the geophysical characteristics of the lithosphere sustainably and that the high porosity of the upper lunar crust is most likely impact induced.

## 1. INTRODUCTION

While the interior of the Moon is comparably homogeneous on global scale, the near-surface crustal structure is complex. In-situ seismic data as well as gravity measurements reveal that compaction of the crustal rocks increases quickly with depth. Also, there is evidence for significant regional variety in upper crust composition and physical properties.

The lunar near-surface structure is of great interest, as it reveals details of early crustal formation from the lunar magma ocean as well as subsequent evolution during the late heavy bombardment. The density may constrain the composition of the upper crust and availability of lunar resources. Besides, bulk density of the upper crust is needed to model mass distribution of the lower crust, independently from topographic features (calculation of Bouguer gravity).

In the past years, techniques have been demonstrated to obtain the density of the lunar crust using gravity data from Gravity Recovery and Interior Laboratory (GRAIL) mission (Zuber et al., 2013) in combination with topography data. Besserer et al. (2014) performed a localized, multitaper spectral analysis on gravity and topography data, to study variations in the vertical density structure. While for the lunar highlands an average increase of density with depth of around 35 kg $m^{-3}$ $km^{-1}$ was found, mare regions reveal dense basaltic material to overly low-density anorthositic rock. Wieczorek et al. (2013) mapped the lateral variations in crustal density by analyzing the correlation between the gravity field and topography. A gravity field model of degree and order 420 was used to produce a crustal density map with a grid of 60 km spacing. Bulk density was found to vary between 2300 and 2900 kg $m^{-3}$ globally. An average bulk density of the Moon's highland crust of 2550 kg $m^{-3}$ was determined, substantially lower than estimated in earlier studies. From bulk density and grain density, the porosity can be determined. Studies by Wieczorek et al. (2013) reveal that the lunar upper crust is highly fractured. An average porosity of 12% was determined, varying between 4 and 21%. A correlation was found between high crustal porosity and the location of large impact basins, which confirms the idea that crustal fracturing is most likely impact induced.

The derived gravity field models from GRAIL are available in an unrivaled resolution and accuracy compared to other planetary bodies. With data from GRAIL's extended mission (Lemoine et al., 2014) and improved processing strategies, gravity field models of the Moon are now available in higher accuracy and resolution. In this study we map bulk density and the porosity of the lunar crust in high spatial resolution, using most recent gravity and topography data. We assume a homogeneous density of the crust in the vertical, as Wieczorek et al. (2013), and seek for lateral variations. In our approach, we benefit from the fact that the measured gravity signal at short wavelengths strongly correlates with the topography (Turcotte and Schubert, 2014). In this paper, we applied two separate methods, not contemplating alone on the correlation between gravity anomalies and the overlying topography, but also on the roughness of the anomalies.

## 2. DATA

We use the gravity field solution GL1500E from data obtained during the primary and the extended GRAIL mission (Park et al., 2015), which is typically given in a series of spherical harmonic coefficients. The relation between the coefficients (frequency domain) and gridded surface data (spatial domain) may be expressed as


https://doi.org/10.5194/isprs-annals-IV-2-W5-527-2019  

$$f(\theta,\phi) = \sum_{l=0}^{\infty}\sum_{m=0}^{l} \bar{P}_{lm}(\cos\theta)(\bar{c}_{lm}\cos m\phi + \bar{s}_{lm}\sin m\phi) \quad (1)$$

where $\bar{c}_{lm}$ and $\bar{s}_{lm}$ are the given $4\pi$ normalized spherical harmonic coefficients of degree $l$ and order $m$, $\bar{P}_{lm}$ are the fully normalized associated Legendre functions, and $\theta$ and $\phi$ colatitude and longitude, respectively (Hofmann-Wellenhof and Moritz, 2005).

GL1500E has a resolution of spherical harmonic degree and order 1500, corresponding to a spatial grid size of around 7 arcminutes or 3.6 km at the equator. To assess the noise level of the dataset, we compute the root mean square (RMS) power spectra of the gravity signal following Kaula (1966) and compare these with the uncertainties, provided for each gravity coefficient (Fig. 1). For degree higher than 910, errors become larger than the power of the signal.

Likewise, we computed the power spectrum of Bouguer anomalies (see explanation later in the text) using a global crustal density of 2550 kg m$^{-3}$ (Wieczorek et al., 2013). The RMS power approaches the GL1500E error near degree 700. Consequently, we decided to truncate the coefficient series at degree and order 700. Also, we removed coefficients smaller than degree 150, to avoid contributions of the crust mantle interface gravity signal (Wieczorek et al., 2013). The remaining set of coefficients is assumed to represent attraction from topography only.

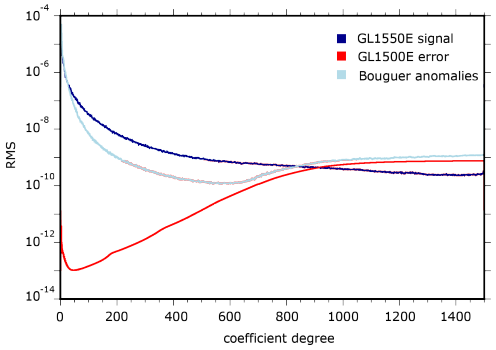


Figure 1. Power spectra of the GRAIL gravity field model GL1500E, the associated uncertainties of the coefficients, and the Bouguer anomalies, calculated with a crustal density of 2550 kg m$^{-3}$

In addition to GRAIL gravity we use the topography from Lunar Orbiter Laser Altimeter (LOLA) (Smith et al., 2017). To match the resolution of the gravity field, we reduced the topography to the same spherical harmonic extension of degree and order 700. Both, topography and gravity field, are given in the principal axis (PA) reference system (NASA, 2008).

## 3. METHOD

To determine crustal density we benefit from the fact that the short wavelength gravity field (corresponding to high degree coefficients) strongly correlates with the topography (Turcotte and Schubert, 2014). From the given topography and some adopted bulk density $\rho$, we compute the Bouguer correction, i.e. the gravity attraction of the terrain related to a certain reference radius. The Bouguer correction was then subtracted from the observed gravity field (truncated to degree and order 150 - 700) to determine the best-fit density $\rho$.

For a given surface point a simple model of the Bouguer correction is the infinite plate of thickness $h$ with constant density $\rho$, where $G$ is the gravitational constant (Hofmann-Wellenhof and Moritz, 2005)

$$g = 2\pi G\rho h \quad (2)$$

however, the method is not applicable if the topography of the surrounding terrain is rough. Instead, the Bouguer correction was calculated applying the finite amplitude method of Wieczorek and Phillips (1998), which – like the observed gravity and topography – may be given in terms of spherical harmonic coefficients, and which may be computed from the expression

$$C_{lm} = \frac{4\pi D^3}{M(2l+1)}\sum_{n=1}^{l+3}\frac{(\rho h^n)_{lm}}{D^n n!}\frac{\prod_{j=1}^{n}(l+4-j)}{(l+3)} \quad (3)$$

where $h$ is the terrain above a reference surface of radius $D$ with a constant density $\rho$ (Wieczorek, 2009). $M$ denotes the mass of the planetary body. To account for the high resolution of our dataset, we estimated coefficients using power series of topography up to $n = 9$.

Bouguer correction was computed for 20 distinct values of densities varying between 2000 and 3000 kg m$^{-3}$. Next, Bouguer correction was applied to the observed gravity field, which was downward continued (free-air correction) to the mean elevation of each analysis region. Subtracting normal gravity, we obtain 20 sets of Bouguer anomalies. Assuming a constant density in the vertical direction the resulting signal would be zero if the correct crustal density was applied. If a wrong density was used, gravity attraction from topography is mapped in the Bouguer anomalies (see sketch in Fig. 2).

The computation of the bulk density was realized in the spatial domain. Hence, topography and the 20 Bouguer anomaly models were converted to spatial grid space. Due to the high degree and order of the data, classical models for the synthesis as e.g. presented by Hofmann-Wellenhof and Moritz (2005) take a large computational effort and may suffer from numerical instabilities (Gruber et al., 2011). The transformation from the spectral domain to a spatial grid was performed using the SHTOOLS archive for Python (Wieczorek and Meschede, 2018). The routine is fast and accurate up to degree 2800 (Wieczorek and Meschede, 2018). We chose a regular sampled grid with equally spaced points in latitude and longitude, that conforms the sampling theorem by Driscoll and Healy (1994). The grid, chosen to match the resolution of the given gravity field, has $2l_{max} + 2$ points in latitude and twice the number in longitude direction, i.e. 3002 x 6004 grid points.

The analysis was carried out over small circular analysis regions with radii of 3.0°. We used the weighted Pearson correlation scheme (Pozzi et al., 2012) to account for distortion of the circular regions with proximity to the poles. Points within the analysis region were weighted regarding their latitudinal position, to compensate for their different contributions.

A significant fraction of around 17% (Head, 1976) of the surface of the Moon is characterized by basaltic mare regions. Since mare basalt deposits were most likely formed by partial melting of lunar upper mantle cumulates (Smith et al., 1970) and therefore do not represent crustal material, we omitted those regions from our analysis. We used maps of lunar maria by Nelson et al. (2014)

to identify and exclude locations, having a contribution of more than 2.5% basalts in the analysis circles.
The uncertainties were estimated by considering the average variation around each individual density value. Since the variation mostly depends on different geological characteristics within the considered region (Besserer et al., 2014), the uncertainties are therefore probably on the pessimistic side.

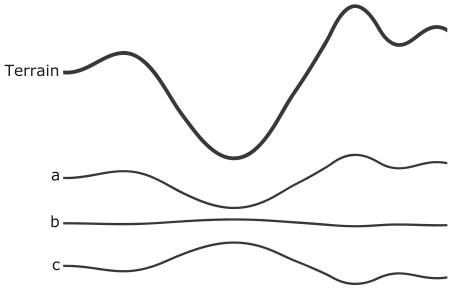


Figure 2. Profiles selected from global data sets, showing topography ("Terrain") and 3 out of 20 Bouguer anomalies, computed using different bulk densities. (a) Applied bulk density too high (b) Applied bulk density just about right. (c) Applied bulk density too low. The best-fit density is found by two different techniques, minimizing the correlation between topography and Bouguer anomalies (sec. 3.1) or by maximizing smoothness of the Bouguer anomalies (sec. 3.2).

### 3.1 Correlation analysis between Bouguer anomalies and topography

The 20 sets of Bouguer anomalies were analyzed to find the best-fit bulk density in each analysis circle using two distinct techniques. Using the technique of Wieczorek et al. (2013), we computed correlation coefficients between Bouguer anomalies and the terrain. Correct crustal density was found where correlation was at a minimum (see Fig. 2 and 3 for sketches).

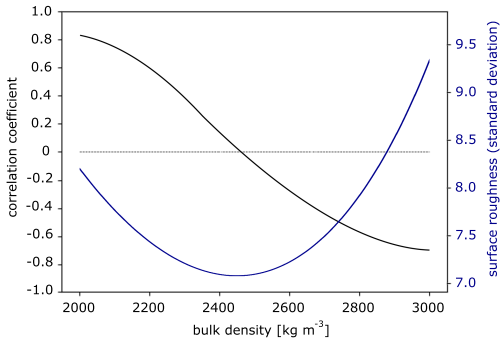


Figure 3. Search for best-fit density for an arbitrary analysis region in the lunar highlands. The black curve shows the determined coefficients of correlation between topography and Bouguer anomalies; best-fit density is found where the curve crosses zero (near 2480 kg m$^{-3}$). The blue curve shows the estimated standard deviations of the Bouguer anomalies; best-fit density is found where standard deviation is smallest (and thus anomaly is smoothest) (near 2460 kg m$^{-3}$).

### 3.2 Roughness of Bouguer anomalies

In the second approach, we computed the standard deviation of the 20 Bouguer anomalies for each analysis circle. Correct density was adopted where standard deviation, i.e., anomaly roughness, was at a minimum (Fig. 2 and 3).

## 4. RESULTS

### 4.1 Bulk density map from correlation analysis

The global bulk density map of the upper lunar crust (Fig. 4) has 480 x 240 grid elements, corresponding to a grid size of 0.75° (approx. 22.5 km at the equator). The map was derived from gravity and topography data as described above, having a spatial resolution of 0.06°.

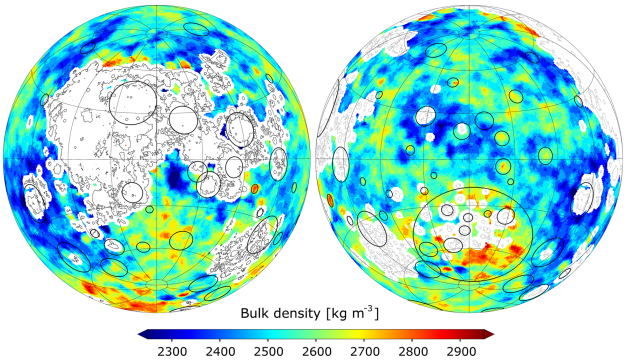


Figure 4. Bulk density of the lunar crust from correlation analysis. The data is mapped in lambert azimuthal equal-area projection, covering a 240° latitude and longitude range (nearside: left; farside: right). Prominent impact basins are marked with black circles. White areas represent lunar maria and are not mapped in our investigation.

Based on degree and order of the truncated spherical harmonic series and the vertical extent of each analysis circle, we estimate bulk density to a depth of several kilometers.
We found an average bulk density of 2536 kg m$^{-3}$ with an uncertainty of ± 21 kg m$^{-3}$. A histogram of globally estimated densities is given in 5A. The majority (99.6%) of determined densities are within a range from 2300 to 2900 kg m$^{-3}$, with only a small number of points beyond.
For estimating the correlation between topography and Bouguer anomalies, we used a circular analysis region of 3° radius for each grid point. For finding the minimum dimension for the analysis circle we tested different radii. Since our estimated errors are influenced by geological characteristics of the investigated region, the uncertainties do not give an indication for the right dimension. Huang and Wieczorek (2012) demonstrated that grain densities of the lunar highlands do not exceed 3000 kg m$^{-3}$. We applied a minimum radius of the analysis circle, where the resulting densities in the highlands remain below the value of 3000 kg m$^{-3}$.

### 4.2 Bulk density from Bouguer anomaly analysis

We tested a modified method, where, instead of examining the correlation between topography and truncated Bouguer anomalies, the roughness of the truncated Bouguer anomalies were considered. We applied the same conditions as in the correlation approach, using circular analysis region of 3.0° radius on a regular grid of 0.75°. An average bulk density of 2503 kg m$^{-3}$ with an uncertainty of ± 22 kg m$^{-3}$ was estimated.
Results for most areas agree with those of the correlation

approach, which supports the validity of the two methods. Overall, the Bouguer roughness approach exhibits slightly lower densities, compared to the correlation approach (Fig. 5). For 3% of the areas on the global map larger differences occur, which will be examined in the discussion section.

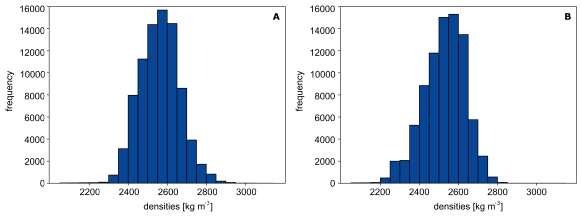


Figure 5. Frequency of the globally determined bulk densities. (A) Histogram of global crustal density estimates from correlation analysis. (B) Histogram of global crustal density estimates from Bouguer anomaly roughness.

### 4.3 Porosity

Porosity is the fraction of the volume made up of pore space (Turcotte and Schubert, 2014). For calculating the porosity, bulk densities as well as the grain densities need to be known. We benefit from the fact that average grain densities of lunar rocks are proportional to abundances of their main chemical constituents. Following Huang and Wieczorek (2012) we used titanium abundances from gamma ray spectrometer data (Prettyman et al., 2006) obtained by the Lunar Prospector mission to map the grain density of the upper crust. The porosity $\phi$ was then determined from the relation

$$\phi = 1 - \frac{\rho_{bulk}}{\rho_{grain}} \quad . \tag{4}$$

Maps were prepared in matching formats as those in Fig. 4. For the highlands upper crust of the Moon an average of 13% porosity for the correlation approach and 14% porosity for the Bouguer roughness approach was determined.

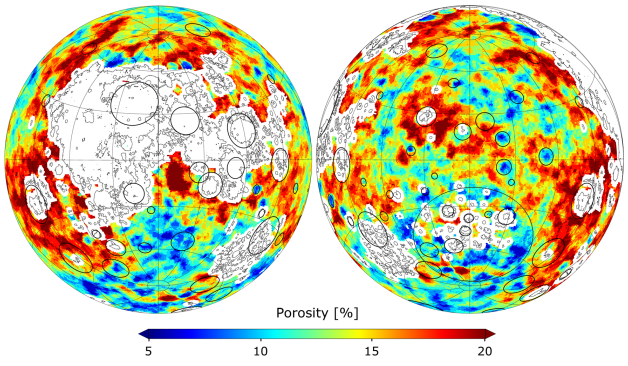


Figure 6. Porosity of the lunar crust (bulk densities were estimated applying the correlation approach). Projection and labels as in Fig. 4.

As it can be seen in Huang and Wieczorek (2012), grain densities are quite similar over the globe, with the only exception of Procellarum KREEP Terrane (PKT). Appart from PKT densities may vary locally only by up to 2%. Therefore, we may conclude that our observed lateral variations in bulk density are mainly induced by the variations in porosity of lunar rock.

## 5. DISCUSSION

Our results agree with those from earlier studies by Wieczorek et al. (2013) and Goossens et al. (2017), who determined an average bulk density of the upper crust of 2550 $\pm$ 18 kg m$^{-3}$ (GL0420A gravity model) and 2587 $\pm$ 54 kg m$^{-3}$ (GRGM900C gravity model), respectively. The porosity of 12% in the study by Wieczorek et al. (2013) is slightly smaller than our estimated average of 13%, using the correlation approach, and 14%, considering the Bouguer anomaly roughness.

The derived maps, showing lateral variations in bulk density and porosity of the upper lunar highland crust, have a resolution two times higher compared to the maps of Wieczorek et al. (2013). Due to the high level of detail we found evidence for significant regional variety in near-surface composition and physical properties. The high-resolution maps reveal a coherence between impact basins and the porosity of the lunar crust.

An example is given in Fig. 7, showing the Korolev farside basin, with a diameter of 417 km (Neumann et al., 2015). Within the inner ring of the basin, the upper crust possesses low porosity of 5%, likely caused by compaction of the target rock and the formation of dense impact melt (Melosh, 1989). In contrast, the region towards the outer rim holds high porosities of around 15%. These areas were probably affected by the shock wave during the contact and compression stage (Melosh, 1989), which caused fracturing and brecciation of the rock (Collins, 2014).

These findings confirm earlier investigations suggesting that impact induced fracturing is the primary mechanism forming the porous upper crust of the Moon and other terrestrial planets (Soderblom et al., 2015; Collins, 2014). The high spatial resolution of the maps will enable further studies focusing on the geophysical characteristics of single impact basins.

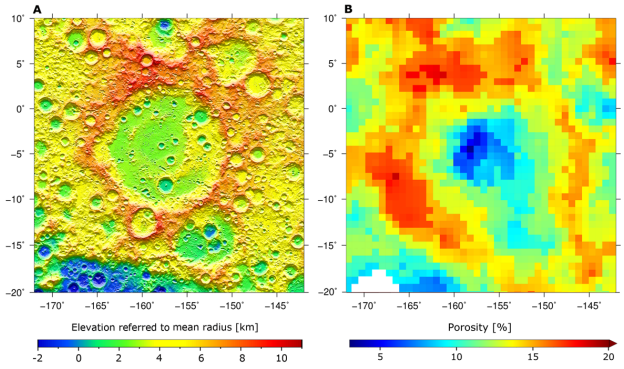


Figure 7. Korolev impact basin. The maps are presented in Mercator projection, with its meridian placed in the center of the basin. (A) Digital terrain model derived from LOLA data (Smith et al., 2017), elevations refer to mean topography radius of 1737.151 km, (B) Porosity of the upper lunar crust.

To obtain the best-fit density, we used two distinct methods. For most areas (97%) results are similar, not different by more than 100 kg m$^{-3}$. However, in particular regions (e.g. at the edge to the Procellarum KREEP Terrane, especially at the northern rim) large differences of up to 700 kg m$^{-3}$ are seen.

To find out the reason for the differences, we mapped topographic roughness, using the standard deviation of topographic data points within the same circular analysis regions, which were used for determining the bulk density. We found that different bulk density solutions are typically found in areas of low surface

roughness. An example is demonstrated in Fig. 8, for a region at the northern boundary of the PKT.
A smooth surface, lacking topographic features, is a challange for both methods. Usually, if a wrong density was applied, surface attributes are mapped in the Bouguer anomalies. The anomalies become rough and a correlation with the topography is found. If topographic features lack, any difference can be made between a wrong and the correct density which was used. The situation is similar for regions of lunar maria: also here topography exhibits only few landforms and craters, so that most of the areas are flat. In the present work, mare regions were omitted from the analysis in particular due to their different composition and origin compared to lunar highland crust (see earlier explanations). But the surface characteristics also make it difficult to achieve meaningful results in those areas.

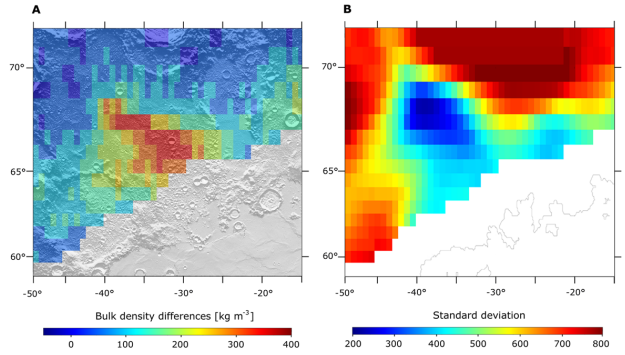


Figure 8. Region of large inconsistence of the two tested methods at the northern rim of PKT. (A) Bulk density difference (bulk density from correlation between topography and Bouguer anomalies minus bulk density from Bouguer roughness) with shaded topography in the background (B) Surface roughness, given as the standard deviation of the topography.

The highest bulk densities can be found in the region of South Pole-Aitken basin (SPA), the oldest impact basin on the Moon (Wilhelms, 1987). With a diameter of about 2400 km (Neumann et al., 2015) it represents the largest impact basin in the solar system. Unfortunateley, SPA shows a number of distinct patches of mare basalts, which were excluded from our mapping, why a statement regarding its properties is only possible to a limited extent. As remote sensing data reveals, SPA exhibits a high abundance in pyroxenes, even though the proportions vary within the basin (Moriarty and Pieters, 2018). This mineral most likely originates from the lower crust and/or upper mantle and has a higher density than the anorthite highland crust (Kiefer et al., 2012), which may explain the high bulk density found in SPA.

## 6. CONCLUSION AND OUTLOOK

We mapped lateral variations of bulk density and porosity of the lunar highland crust using most recent high-resolution GRAIL gravity and LOLA topography data. For calculating the density, two methods were demonstrated, both of which yield similar results for most of the studied areas. Both methods suffer in the case of a smooth topography. Consequently, the two methods show significantly different results of up to 700 kg m$^{-3}$ in such areas.
Using global grain densities derived from remote sensing data, we also estimated the porosity of the upper lunar crust. From inspection of the data, we conclude, that differences in the bulk density are mostly determined by differences in crustal porosity, not by differences in the statistics of chemical compounds. We demonstrate that high porosity correlates with areas around impact basins, which suggests that the fracturing is most likely impact-induced.
With the present high-resolution datasets, it is possible to study impact structures in more detail. We will take a closer look at single basins regarding their variations in porosity and investigate their characteristics in terms of dimension and age.
Accurate bulk densities near the surface are important for studies of deeper crustal structures. Rather than using one average value, the high-resolution bulk density maps can be used to calculate mass variations at the crust-mantle boundary with individual values for different areas.

## ACKNOWLEDGEMENTS

We gratefully acknowledge Mark Wieczorek for helpful discussions and advice. We also would like to thank two anonymous reviewers for critical comments and suggestions, which helped improving the manuscript. This work was funded by the Deutsche Forschungsgemeinschaft (SFB-TRR 170, subproject A04-60).

## REFERENCES

Besserer, J., Nimmo, F., Wieczorek, M. A., Weber, R. C., Kiefer, W. S., McGovern, P. J., Andrews-Hanna, J. C., Smith, D. E. and Zuber, M. T., 2014. GRAIL gravity constraints on the vertical and lateral density structure of the lunar crust. *Geophysical Research Letters* 41(16), pp. 5771–5777.

Collins, G. S., 2014. Numerical simulations of impact crater formation with dilatancy. *Journal of Geophysical Research* 119(12), pp. 2600–2619.

Driscoll, J. R. and Healy, D. M., 1994. Computing fourier transforms and convolutions on the 2-sphere.

Goossens, S., Sabaka, T. J., Genova, A., Mazarico, E., Nicholas, J. B. and Neumann, G. A., 2017. Evidence for a low bulk crustal density for Mars from gravity and topography. *Geophysical Research Letters* 44(15), pp. 7686–7694.

Gruber, C., Novák, P. and Sebera, J., 2011. Fft-based high-performance spherical harmonic transformation. *Studia Geophysica et Geodaetica* 55(3), pp. 489–500.

Head, J. W., 1976. Lunar volcanism in space and time. *Reviews of Geophysics and Space Physics* 14(2), pp. 265–300.

Hofmann-Wellenhof, B. and Moritz, H., 2005. *Physical Geodesy*. Springer-Verlag, Wien.

Huang, Q. and Wieczorek, M. A., 2012. Density and porosity of the lunar crust from gravity and topography. *Journal of Geophysical Research E: Planets* 117(5), pp. 1–9.

Kaula, W., 1966. *Theory of Satellite Geodesy*. Blaisdell Puplishing Company, Waltham, Mass. (republished by Dover, New York, 2000).

Kiefer, W. S., Macke, R. J., Britt, D. T. and Irving, A. J., 2012. The density and porosity of lunar rocks. *Geophysical Research Letters* 39, pp. 1–5.

Lemoine, F. G., Goossens, S., Sabaka, T. J., Nicholas, J. B., Mazarico, E., Rowlands, D. D., Loomis, B. D., Chinn, D. S., Neumann, G. A., Smith, D. E. and Zuber, M. T., 2014. GRGM900C: A degree 900 lunar gravity model from GRAIL primary and extended mission data. *Geophysical Research Letters* 41(10), pp. 3382–3389.

Melosh, H. J., 1989. *Impact cratering: A Geologic Process*. Oxford University, New York.

Moriarty, D. P. and Pieters, C. M., 2018. The Character of South Pole-Aitken Basin: Patterns of Surface and Subsurface Composition. *Journal of Geophysical Research: Planets* 123, pp. 729–747.

NASA, 2008. *A Standardized Lunar Coordinate System for the Lunar Reconnaissance Orbiter and Lunar Datasets*. Vol. 5, NASA Goddard Space Flight Center, Greenbelt, Md.

Nelson, D. M., Koeber, S. D., Daud, K., Robinson, M. S., Watters, T., Banks, M. and Williams, N. R., 2014. Mapping Lunar Maria Extents and Lobate Scarps Using LROC Image Products. *Lunar and Planetary Science Conference*.

Neumann, G. A., Zuber, M. T., Wieczorek, M. A., Head, J. W., Baker, D. M. H., Solomon, S. C., Smith, D. E., Lemoine, F. G., Mazarico, E., Sabaka, T. J., Goossens, S. J., Melosh, H. J., Phillips, R. J., Asmar, S. W., Konopliv, A. S., Williams, J. G., Sori, M. M., Soderblom, J. M., Miljković, K., Andrews-Hanna, J. C., Nimmo, F. and Kiefer, W. S., 2015. Lunar impact basins revealed by Gravity Recovery and Interior Laboratory measurements. *Science Advances* 9(1), pp. 1–10.

Park, R. S., Konopliv, A. S., Yuan, D., Asmar, S., Watkins, M., Williams, J., Smith, D. and Zuber, M., 2015. A high-resolution spherical harmonic degree 1500 lunar gravity field from the grail mission. *AGU Fall Meeting Abstracts* pp. G41B–01.

Pozzi, F., Di Matteo, T., and Aste, T., 2012. Exponential smoothing weighted correlations. *European Physical Journal B* 85(6), pp. 1–21.

Prettyman, T. H., Hagerty, J. J., Elphic, R. C., Feldman, W. C., Lawrence, D. J., McKinney, G. W. and Vaniman, D. T., 2006. Elemental composition of the lunar surface: Analysis of gamma ray spectroscopy data from Lunar Prospector. *Journal of Geophysical Research E: Planets* 111(12), pp. 1–41.

Smith, D. E., Zuber, M. T., Neumann, G. A., Mazarico, E., Lemoine, F. G., Head, J. W., Lucey, P. G., Aharonson, O., Robinson, M. S., Sun, X., Torrence, M. H., Barker, M. K., Oberst, J., Duxbury, T. C., Mao, D., Barnouin, O. S., Jha, K., Rowlands, D. D., Goossens, S., Baker, D., Bauer, S., Gläser, P., Lemelin, M., Rosenburg, M., Sori, M. M., Whitten, J. and Mcclanahan, T., 2017. Summary of the results from the lunar orbiter laser altimeter after seven years in lunar orbit. *Icarus* 283, pp. 70–91.

Smith, J. V., Anderson, A. T., Newton, R. C., Olsen, E. J., Crewe, A. V., Isaacson, M. S., Johnson, D. and Wyllie, P. J., 1970. Petrologic history of the moon inferred from petrography, mineralogy and petrogenesis of apollo 11 rocks. *Geochimica et Cosmochimica Acta Supplement, Volume 1. Proceedings of the Apollo 11 Lunar Science Conference held 5-8 January, 1970 in Houston, TX.: Mineraolgy and Petrology. Edited by A. A. Levinson. New York: Pergammon Press, 1970.* 1, pp. 897–925.

Soderblom, J. M., Evans, A. J., Johnson, B. C., Melosh, H. J., Miljkovi, K., Phillips, R. J., Andrews-hanna, J. C., Bierson, C. J., Iii, J. W. H., Milbury, C., Neumann, G. A., Nimmo, F., Smith, D. E., Solomon, S. C. and Sori, M. M., 2015. The fractured Moon: Production and saturation of porosity in the lunar highlands from impact cratering. pp. 6939–6944.

Turcotte, D. and Schubert, G., 2014. *Geodynamics, 3rd edition*. Cambridge University Press, Cambridge.

Wieczorek, M. A., 2009. Gravity and topography of the terrestrial planets. In: G. Schubert and T. Spohn (eds), *Treatise on Geophysics*, Vol. 10, Elsevier, Amsterdam, pp. 165–206.

Wieczorek, M. A. and Meschede, M., 2018. SHTools: Tools for Working with Spherical Harmonics. *Geochemistry, Geophysics, Geosystems* 19(8), pp. 2574–2592.

Wieczorek, M. A. and Phillips, R. J., 1998. Potential anomalies on a sphere: Applications to the thickness of the lunar crust. *Journal of Geophysical Research* 103(97), pp. 1715–1724.

Wieczorek, M. A., Neumann, G. A., Nimmo, F., Kiefer, W. S., Taylor, J. G., Melosh, H. J., Phillips, R. J., Solomon, S. C., Andrews-Hanna, J. C., Asmar, S. W., Konopliv, A. S., Lemoine, F. G., Smith, D. E., Watkins, M. M., Williams, J. G. and Zuber, M. T., 2013. The Crust of the Moon as Seen by GRAIL. *Science* 339, pp. 671–675.

Wilhelms, D. E., 1987. The geological history of the Moon.

Zuber, M. T., Smith, D. E., Watkins, M. M., Asmar, S. W., Konopliv, A. S., Lemoine, F. G., Melosh, H. J., Neumann, G. A., Phillips, R. J., Solomon, S. C., Wieczorek, M. A., Williams, J. G., Goossens, S. J., Kruizinga, G., Mazarico, E., Park, R. S. and Yuan, D.-n., 2013. Gravity Field of the Moon from the Gravity Recovery and Interior Laboratory (GRAIL) Mission. *Science* 339, pp. 2011–2014.